Fusion Engineering and Design 204 (2024) 114469

Contents lists available at ScienceDirect

Fusion Engineering and Design

journal homepage: www.elsevier.com/locate/fusengdes

Development of SPARC plasma disruption database through electromagnetic predictive MAXFEA modelling

M. Scarpari [a,*], R. Lombroni [a], A. Mele [a], S. Carusotti [a], S. Minucci [a], G. Liuzzo [a], M. Notazio [a], V. Riccardo [b], G. Calabrò [a], P. Fanelli [a]

[a] Department of Economy, Engineering, Society and Business Organization (DEIM), University of Tuscia (UNITUS), Largo dell'Università, Viterbo 01100, Italy
[b] Commonwealth Fusion Systems (CFS), Cambridge, MA 02139, USA

ARTICLE INFO

Keywords:
SPARC
Disruptions loads
VDE
MAXFEA
Synthetic experiments
Synthetic Displacements Diagnostic

ABSTRACT

The evaluation of electromagnetic (EM) behaviour of tokamak components under disruption loads and its correlation with vertical instabilities is critical and characterizing the design considerations. This is particularly crucial for high-field and burning plasma experiments such as the SPARC tokamak, the compact prototype currently under construction by Commonwealth Fusion Systems (CFS). The combination of high toroidal magnetic field (12.2 T) and high plasma current (8.7 MA) makes SPARC less tolerant to disruptions than currently operating research devices. In this context, recent efforts have been made to characterize the disruption loads in SPARC by conducting a series of analyses to estimate the EM response of the SPARC vacuum vessel (VV) during a plasma vertical displacement event (VDE). In this paper, the aforementioned analyses are used as starting point for a comprehensive characterization of VDE scenarios. These analyses are utilized to create a database of predictive disruption simulations, serving as synthetic experiments to generate and collect pertinent data for upcoming research studies. In this context, the paper discusses a preliminary description of an innovative VV synthetic displacements diagnostic, designed starting from disruption database, presented here, and by exploiting the MAXFEA-ANSYS combined use methodology as further step. The disruptive plasma scenarios database will be functional in estimating the displacement and strain fields of SPARC components using a limited set of VV indirect displacement measurements and integral plasma observations, such as plasma current and effective plasma position.

1. Introduction

SPARC stands for the smallest/soonest as possible, affordable, robust, compact (ARC [1]) reactor. SPARC is a tokamak designed by CFS, a privately funded company, and the Massachusetts Institute of Technology (MIT), a non-profit university. SPARC is expected to operate at high performance levels in terms of plasma current and magnetic field. Under such conditions, which are similar to those expected in future tokamak-based power plants, much lower tolerances for plasma instabilities and disruptions are anticipated compared to present research devices [2,3]. The acceptable frequency of these events is quantified by the economic impact they have on power production and on machine maintenance and downtime. Recently, a set of analyses to estimate the EM response of the SPARC VV during a VDE was carried on and reported in [4], where different scenarios were considered to characterize the disruption loads. Other considerable studies on the physics of SPARC disruptions can be found in [2] and [5], where investigations on the natural disruption physics expected in SPARC are detailed. However, the literature on SPARC disruptions that specifically targets a comprehensive assessment of EM loads for engineering purposes remains limited. The perspective of employing detailed Finite Element Method (FEM) modelling to delve into SPARC disruption plasma dynamics across varied spatial parameters is presently underexplored.

Starting from the aforementioned studies on SPARC disruptions, this paper discusses the use MAXFEA code, a 2D evolutionary equilibrium procedure [6,7], to exploit a large set of disruption scenarios for SPARC tokamak. MAXFEA has recently undergone extensive validation and verification activities against both experimental data and other predictive methodologies, as discussed in [8,9]. Similarly to those previous work, a detailed and self-consistent disruption simulation database (DB), has been constructed and will be presented here. Since MAXFEA is

* Corresponding author.
E-mail address: mattia.scarpari@unitus.it (M. Scarpari).

https://doi.org/10.1016/j.fusengdes.2024.114469
Received 12 October 2023; Received in revised form 5 April 2024; Accepted 22 April 2024
Available online 7 May 2024

a 2D axisymmetric procedure, the evaluation of 3D effects (i.e. local current and forces concentrations) is not covered in this context. However, it should be noted that this paper is intended to be an initial study in fully specifying VDE loads from both EM and structural perspectives (see Fig. 1). Next steps will provide a complete loads specification, as detailed in [10,11,12]. Considering these factors, the significance of this study lies in addressing the deficiency in precise FEM modelling of SPARC disruption plasma dynamics, while systematically exploring various parameters of interest.

Indeed, the ultimate objective of the present work, as shown in Fig. 1, is to develop a 3D SPARC synthetic VV deformations diagnostic by exploiting the MAXFEA-ANSYS combined use methodology, presented in [7,13,14,15]. This methodology aims to estimate displacement and strain field calculations, based on the VDE DB results, ultimately leading to stress measurements that characterize the SPARC VV. With synthetic diagnostics, the term refers to all those “indirect” measurements of displacement and strain field of components, which, under the assumption of small displacements and elastic, isotropic, and homogeneous behaviour, translate into immediate measurements of stress. Indeed, it can be conceptualized as an "indirect" or synthetic measurement based on numerical calculation, rather than direct diagnostic and experimental measurement. The goal is to design and optimize the position of displacement or deformation synthetic sensor at limited accessible points of the vacuum vessel. However, their positioning is determined by access constraints, and their quantity is limited by budget considerations. The establishment of the proposed numerical disruption database and the resulting 3D EM loads, extrapolated from collected and accurate plasma dynamics, possibly using machine learning (ML) models, will facilitate the development of modal reconstruction algorithms [16] for the selection of vibration modes.

The paper is organized as follows. Section 2 deals with the description of the components included into the numerical model with the focus on SPARC plasma equilibrium reconstruction. This section also contains a study on the calculation of the growth rate (GR) for the characterization of the SPARC plasma vertical instability, performed through a simplified RZIp model [17]. Section 3 shows the proposed predictive methodology applied to SPARC and the respective outcomes in terms of plasma evolution and 2D EM loads, starting from the evidence provided in [4,18]. Finally, Section 4 deals with the construction of the predictive disruption simulation DB providing a large case of numerical VDEs for SPARC which will constitute the starting point for the subsequent work on VV deformation synthetic diagnostic.

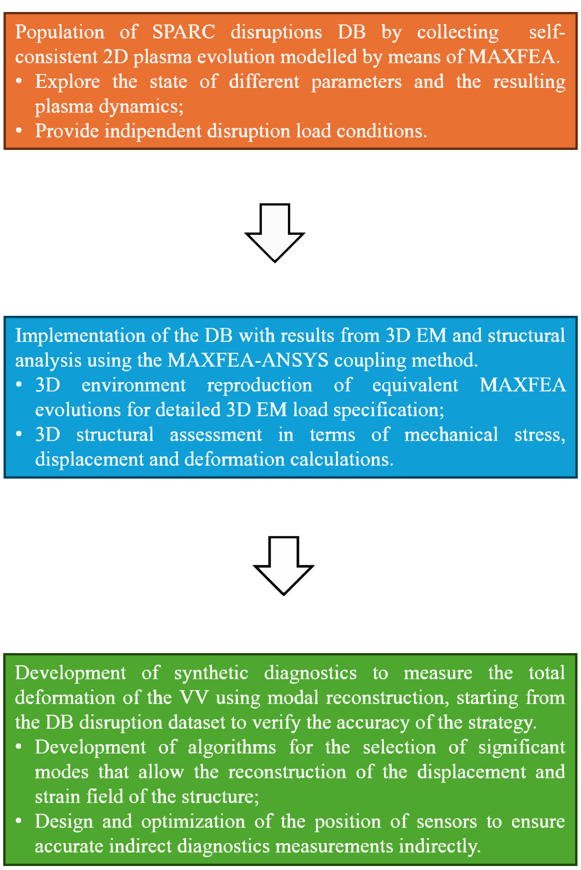

Fig. 1. Flowchart of the proposed procedure from the 2D disruption DB to the development of synthetic diagnostics.

2. 2D SPARC numerical model description

The proposed approach relies on the use of SPARC 2D axisymmetric MAXFEA FEM model for the disruption modelling. Concerning the main components of SPARC, the entire SPARC device is up–down symmetric, enabling symmetric double null (DN) operation (see Fig. 2). It can be seen in Fig. 2a, the VV has three ports at each toroidal location, one midplane port and a symmetric pair of off-midplane ports above and below [19]. Fig. 2b shows the poloidal cross-section of SPARC and the coils system. Central solenoid consists of a total of three pairs of high temperature superconducting upper and lower coils, labelled CS1, CS2 and CS3 [19]. The machine has four upper and lower pairs of high temperature superconductor (HTS) poloidal field coils (PF) outside of the toroidal field coils (TF), labelled PF1 to PF4, moving outward in major radius. In addition, there are two pairs of copper coils that are internal to the toroidal field coils but external to the vacuum vessel [19]. Since these coils are primarily used to actuate the divertor magnetic field, they are labelled DIV1 and DIV2 upper and lower. These pair of coils are covered by a SS316 casing (again upper and lower). Finally, there is also a pair of vertical stability coils inside of the VV, labelled VS1 upper and lower [19].

2.1. MAXFEA model and equilibrium reconstruction

The SPARC MAXFEA numerical model includes the following components:

- Vacuum vessel made of Nitronic-50 at 75 °C (magenta and dark blue areas in Fig. 3a), with ports modelled as equivalent resistivities calculated via a full-empty ratio in terms of volume to take into account the toroidal discontinuity of the vessel in those areas (black dashed areas in Fig. 3a);

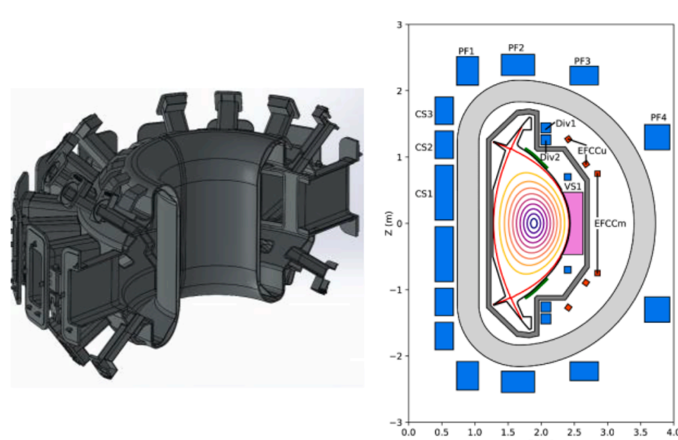

(a) (b)

Fig. 2. SPARC components Overview: a) 180° of CAD view of SPARC VV. b) SPARC poloidal cross-section [19].

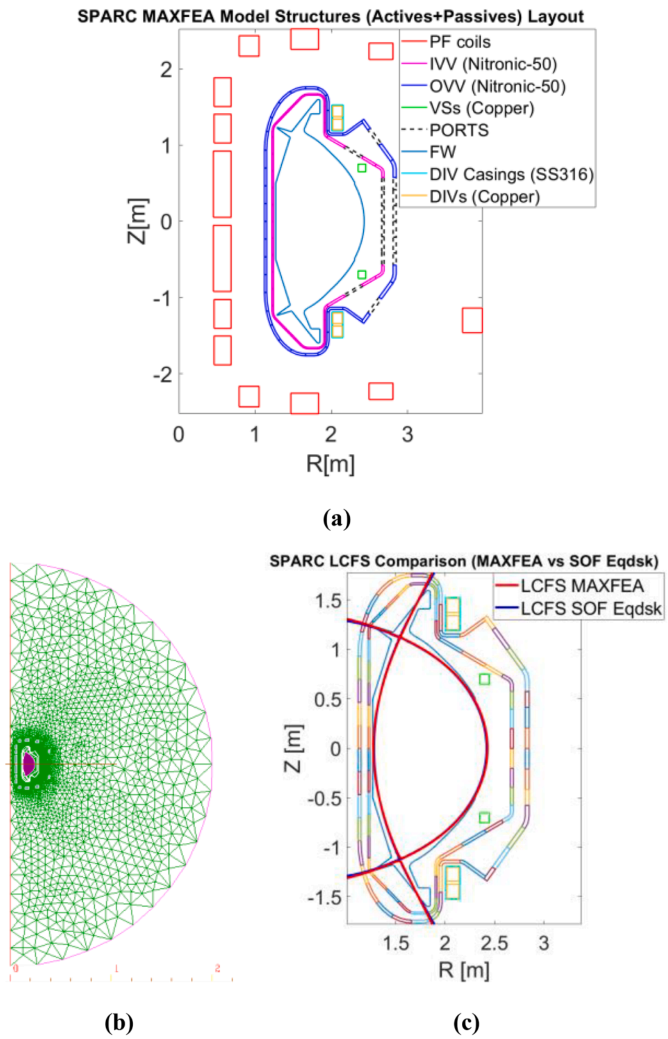

Fig. 3. SPARC MAXFEA model and reproduction of starting equilibrium: a) Overview of the model. The PF coils are represented in red. The VV and the port areas are represented in magenta-blue and in black respectively. DIV and VS coils are represented in green and yellow respectively. The DIV casings are in cyan, and the first wall is in blue. b) The MAXFEA triangular mesh is reported. c) The equilibrium reproduced by means of MAXFEA is reported in red, blue for the reference one.

- PF coils represented by red areas in Fig. 3a;
- VS coils (green areas in Fig. 3a) modelled as copper short-circuited coils with a top-bottom anti-series connection (6 turns each);
- DIV coils (yellow areas in Fig. 3a) as independently supplied copper circuits (24 turns each) covered by a couple of casings made of SS316 (cyan areas in Fig. 3a);
- The divertor and first wall limiting surfaces are reported in blue (see Fig. 3a).

Expanding upon the premise in the first point. The model developed is an axisymmetric 2D model, and the objective is to obtain an equivalent plasma response. There are several methodologies to account for this approximation and attempt to replicate the effect of real 3D structures on the axisymmetric mode ($n = 0$), which are discussed in detail in [20]. The increase in resistivity based on the empty-full ratio for the ports is a first-order approximation to try to better retain the equivalent response of passives on the plasma. In addition, all the structures characterized by negligible effects in terms of poloidal field variation loads or plasma dynamic behaviours are neglected (such as purely toroidally discontinuous structures or components with small poloidal cross-section).

An overview of the model is reported in Fig. 3 together with an example of equilibrium reconstruction. The starting DN plasma equilibrium reproduced with MAXFEA is shown in Fig. 3c in terms of last closed flux surface (LCFS), together with the reference LCFS provided at start of flat top condition.

Table 1 shows the main equilibrium plasma parameters that characterize the DN configuration of SPARC reconstructed equilibrium.

The comparison between the two LCFSs of Fig. 3c shows a qualitative good agreement. Nonetheless, the model can be considered benchmarked in terms of the starting equilibrium, as it achieves similar values for plasma shape and internal plasma parameters compared to the reference data provided [18].

2.2. Preliminary vertical instability analysis applied to 2D SPARC model

To validate the SPARC model from a vertical instability point of view, a benchmark is reported with an implementation of a simplified rigid displacement model (RZIp formulation) for the growth rate calculation [17]. It is a well-known fact that elongated plasma configurations in tokamaks are vertically unstable [21]. In this sub-section the so-called RZIp model, where vertical and radial movements are considered, together with variations of the total plasma current is described and used to analyse such instability. The model takes into account the current distribution of the plasma, assuming rigid displacements of the reference equilibrium configuration. The fundamental idea behind this model is to average the forces acting on the plasma over the considered current distribution. In the model of this unstable vertical motion, the plasma ring is approximated by a rigid filament carrying the total plasma current ($I_{pla,}$). The radius of this filament is denoted by r_p and its vertical position by z_p. The following equations can be considered:

$$L_c \frac{d}{dt}(I_c) + R_c I_c + \psi_{cp} = V_c \tag{1}$$

$$2\pi r_p I_{pla} \langle B_r^{ext}(r_p, z_p, I_c) \rangle = 0 \tag{2}$$

$$2\pi r_p I_{pla} \langle B_z^{ext}(r_p, z_p, I_c) \rangle + F_r(r_p, I_{pla}) = 0 \tag{3}$$

$$\frac{d}{dt}\left[L_p(r_p) I_{pla}\right] + R_p I_{pla} + \psi_{cp} = 0 \tag{4}$$

where $I_c = [I_a I_e]^T$ collects both the active and passive currents, V_c are the corresponding applied voltages (equal to zero for the passive currents) and R_c, L_c are their resistance and mutual inductance matrices respectively. Similarly, the plasma current is denoted by I_{pla} and R_p, L_p are the plasma resistance and self-inductance (the latter depends on the radial position of the filament representing the plasma). ψ_{cp} is the flux contribution from the plasma to the active and passive circuits, $\langle B_r^{ext} \rangle$ and $\langle B_z^{ext} \rangle$ are the radial and vertical field components due to the external circuits averaged over the considered current distribution and F_r is the radial force acting on the plasma. Since the instability is linked to the gradient of the B_r field along the vertical direction, it is standard practice to define the radial field decay index n:

$$n := -\frac{r_p}{B_V} \frac{\partial B_r}{\partial z_p} \tag{5}$$

Table 1
Main SPARC equilibrium plasma parameters referring to the start of flat-top: plasma current (I_{pla}), poloidal Beta (β_p), plasma internal inductance (li), toroidal field at machine radius (B_t at R_0), safety factor (q_{95}), Z and R coordinates of magnetic axis (Z_{maxis} and R_{maxis}).

I_{pla}	β_p	li	B_t at R_0	q_{95}	Z_{maxis}	R_{maxis}
8.7 MA	~0.2	~1	12.2 T (R_0=1.85 m)	~3	~0 m	~1.89 m

where B_V is the vertical field needed to fulfill the radial force balance condition, which we assume to be known (see [22] for more details). The model was used to estimate the growth rate of the DN plasma configuration of SPARC shown in Fig. 3c, obtained through the MAXFEA equilibrium code. In the analysis, the passive elements and the PF coils of the MAXFEA model were approximated with filamentary currents placed in their barycentre, and their mutual inductances were computed numerically through the associated Green functions and validated against the values generated by MAXFEA. The radial field decay index map and the vertical force distribution over the considered plasma current density are reported in Fig. 4a and 4b respectively.

The growth rate outcoming from this analysis is 28.7 s^{-1} resulting in a good agreement with the computed MAXFEA GR $\sim$32 s^{-1}. The obtained results should also be interpreted positively, given their proximity in order of magnitude to the GR obtained from previous SPARC disruption studies, which falls in the range between $50 - 62.5$ s^{-1}, with a best fit of 53 s^{-1} [4,18]. However, slight differences are expected when employing different methodologies and varying the accuracy of the assumptions adopted. Therefore, the 2D SPARC model can be considered well-developed from the perspective of vertical instability and plasma equilibrium conditions.

3. First disruptions MAXFEA modelling approach on SPARC

This section presents the first step of the proposed numerical modelling strategies applied to SPARC. The aim is to utilize evidence observed in previous studies on SPARC perturbations [2,4] to derive accurate numerical disruption scenarios, particularly focusing on plasma dynamics and providing an initial assessment of resulting 2D EM loads. Upon successful application of the modelling strategy to SPARC, exploration of different space parameters was conducted with the goal of populating the database with various synthetic disruptions (Section 4).

3.1. Disruption modelling methodology

The first disruption scenario considered is the upward VDE (UVDE) type characterized by a slow current quench phase [4,18]. Relevant insights can be extrapolated from previous studies on SPARC disruptions. Indeed, as outlined in [2,4], SPARC in-vessel components have been designed to withstand the fastest current quench (CQ), of about 3.2 ms, accordingly to ITPA disruption database scaling [23]. Conversely, VV system is designed to withstand the slowest CQ ($\sim$40 ms) as scaled from experimental observations in the JET-ILW [4,24,25]. It should be noted that the value characterizing the CQ duration for slow events may be difficult to confirm/document. However, it is common practice in the design of various machines, such as DTT [13], to designate a slow CQ duration approximately ten times longer than that allocated for fast events.

In this context, CQ was triggered immediately after the thermal quench (TQ) phase, when the plasma loses its thermal energy by disrupting during the vertical displacement phase [23]. The duration of TQ phase typically ranges from a few to tens of milliseconds, during which up to 50 % of the thermal energy is dissipated. TQ can manifest either in two distinct stages or as a single rapid collapse, known as fast quench. An empirical scaling for the duration of TQ is provided in [23], demonstrating that the duration of the fast quench scales approximately with the plasma minor radius. Nevertheless, the large scatter of experimental data recommends an uncertainty factor from 1/3 to 3 (i.e. for DEMO the total duration of TQ is $\sim 10 - 100$ ms and the fast TQ is $\sim 0.3 - 3$ ms with $a = 2.9$ m). The fast phase of the TQ for SPARC should have a duration of $\sim$0.1 ms [2]. However, despite the complexity and variability of the dynamics of the TQ observed experimentally, in this kind of simulation it is a common practice to assume that all the plasma energy is lost during a single fast phase [7,13,14]. Moreover, it is worth saying that the actual duration of the TQ has a slight effect on the EM simulations, because it is shorter than the vessel resistive time and of the same order of the usual cycle time step.

In the simulation procedure for VDEs modelling, the parameter q_{cyl} serves as the trigger for TQ. Establishing both the upper and lower bounds for q_{cyl} involves making assumptions. For the lower bound, reference can be made to [26], where a critical value of $q_{95} = 1.5$ is assumed, below which plasma magnetohydrodynamic stability is deemed to be severely compromised (note that q_{95} and q_{cyl} have different but similar definitions). However, in the case of SPARC, an even more conservative approach is adopted, setting the lower limit for $q_{cyl} = 1$ [4,18]. It is essential to note that while this scenario is highly improbable, this choice is justified to ensure a conservative assessment of the total vertical force. Therefore, in the proposed simulation, TQ is initiated when the plasma safety factor reaches a value of q_{cyl} approximately equal to 1 (see Table 2). The final phase of TQ for SPARC has a

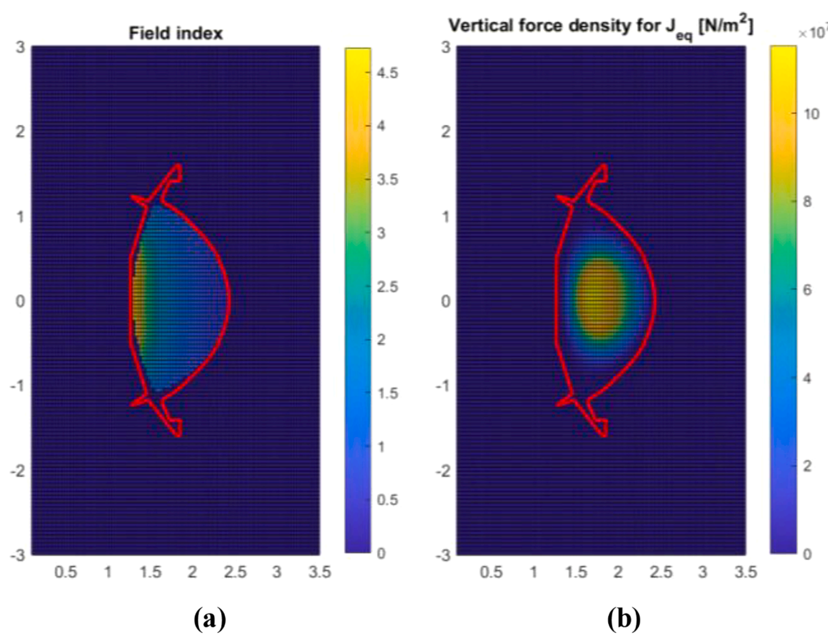

Fig. 4. Radial field decay index map (a). Force density on the considered plasma current distribution (b).

Table 2
UVDE Case 1 and Case 2 modelling methodology.

Case 1	Case 2
1) Destabilizing kick at 1 ms after the start of the simulation to force plasma movement starting from $I_{pla} = 8.7$MA [7]	
2) Flux Normal Mode:	**2) Flux Cons. Mode:**
• Plasma current keep constant until TQ • TQ when Plasma reaches given q_{cyl} ($\simeq$1) as β_p drop ($\Delta tTQ \simeq 0.1$ ms) [4,7,18]	• Plasma current slowly decreasing until TQ • TQ when Plasma reaches given q_{cyl} ($\simeq$1) as β_p drop ($\Delta tTQ \simeq 0.1$ ms) [4,7,18]
3) CQ immediately after TQ, imposing negative voltage on Plasma ($\Delta tCQ \simeq 40$ ms) [4,7]	
4) halo currents growth during CQ phase (halo current fraction: 50 % of I_{pla}) [4,18]	

duration of approximately 0.1 ms (see Table 2), and it is the only TQ phase considered for the simulations as discussed above.

To investigate various conditions during the vertical displacement phase and enhance the comprehensiveness of the information, two preliminary simulations of UVDE with slow CQ were conducted in MAXFEA. These simulations involved different modelling approaches for the VDE phase and were considered as initial cases:

- Case 1: plasma current is kept constant up to TQ (flux normal mode in Table 2);
- Case 2: plasma current is characterized with a certain decreasing time evolution up to TQ computed by the code, imposing a specific magnetic flux conservation condition (flux conservation mode in Table 2).

These two simulative assumptions have an intrinsic influence on the dynamics of the plasma during the VDE. The rationale behind this choice is as follows: during experimental VDE when a vertical instability arises in the plasma, causing it to start moving vertically, the mutual and self-inductance of the plasma change. During the flat-top phase of the scenario, the control system attempts to compensate and maintain the current at the reference value. In absence of specific indication to what would happen in SPARC during this phase, these can be considered as two extremal cases, as one might anticipate that the plasma current evolution in the real world falls somewhere between these two extremes. Taking into account the preceding discussion, the assumptions related to the disruption modelling for the two preliminary cases are consolidated and presented in Table 2.

The main modelling observations from MAXFEA simulations are reported in Fig. 5.

The plasma current evolution (depicted with blue curve) for Case 1 is reported in Fig. 5a, while for Case 2 see Fig. 5b. In an initial phase of the scenario, when the plasma is moving upward before it touches the wall, a constant current trend is observed according to the flux normal mode adopted for Case 1. On the other hand, in Case 2 there is a current reduction due to the flux conservation assumption. In both cases, at a certain point, the plasma touches the wall and TQ (identified with left black vertical line) is imposed when $q_{cyl} \sim 1$ (cyan trends) at ~0.43 s for Case 1 and at ~0.28 s for Case 2. When TQ is imposed, in both cases a current spike is found due to the flux condition and the sudden redistribution of the plasma current, as expected from the experimental evidence [6,11]. CQ takes place immediately after and ends at ~0.47 s in Case 1 and at ~0.32 s in Case 2 (right black vertical line). During the CQ phase, halo currents arise as shown with the red curve, reaching a peak of about 4.3 MA for both cases in accordance with the halo current assumption (see Table 2). It is possible to observe that in Case 2, the plasma disrupts earlier due to the higher instability during vertical displacement compared to the Case 1. This pertains to the variation of the plasma current before TQ occurs, attributed to the discussed different approach employed for the VDE phase.

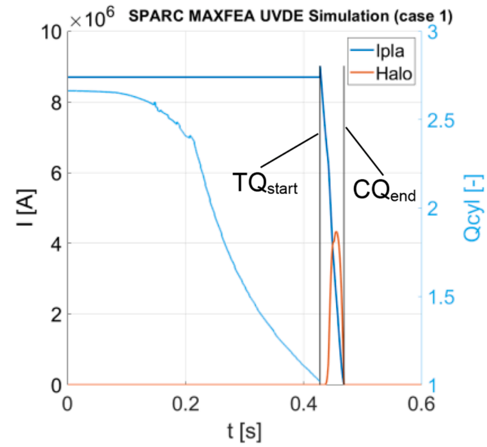

(a)

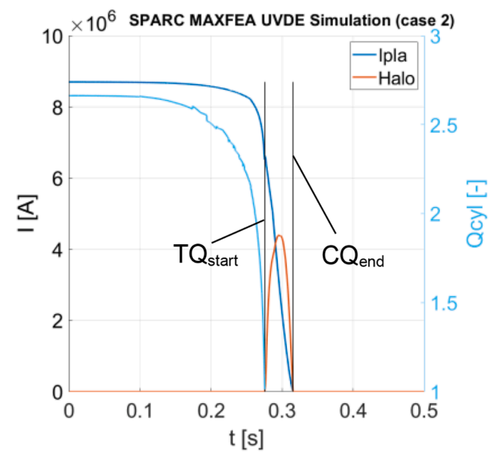

(b)

Fig. 5. main curves from disruptions simulated via MAXFEA for Case 1 (a) and Case 2 (b): both plasma current evolutions and halo current curves are reported (blue curve and red curve respectively, refer to left ordinate axis) and q_{cyl} trends (cyan curve, refers to right ordinate axis). Vertical black lines are referred to the different phases.

3.2. Predictive outcomes

Simulation results in terms of eddy currents, global EM vertical forces on the components, and plasma movement considering Case 1 and Case 2 are reported in this subsection.

Plasma centroid trajectories in time and on poloidal plane are shown in Fig. 6 for both cases, together with the plasma boundary evolution at characteristic times during the event. It is evident that in Case 1 (Fig. 6a1-6a2), the plasma exhibits higher velocity during the displacement phase, reaching close to the first wall contact at around ~0.22 s. The plasma vertical displacement at the onset of TQ is approximately 0.2 m.

Whereas, in the last phase of the vertical displacement, plasma in Case 2 (Fig. 6b1-6b2) is the fastest one due to the increasing of the dynamic effects of the plasma current variation that makes plasma more unstable. In Case 2, the plasma moves vertically with a displacement of about 0.6 m at TQ. This effect may be explained by considering that the contribution of the magnetic field variation due to the faster displacement and the steeper current derivate generate mutual EM effects that accelerate the plasma of Case 2 in the time range between ~0.25 s (first touch with the wall) and ~0.28 s (TQ start). The disparity between the two cases is anticipated due to distinct evolutions in magnetic flux and

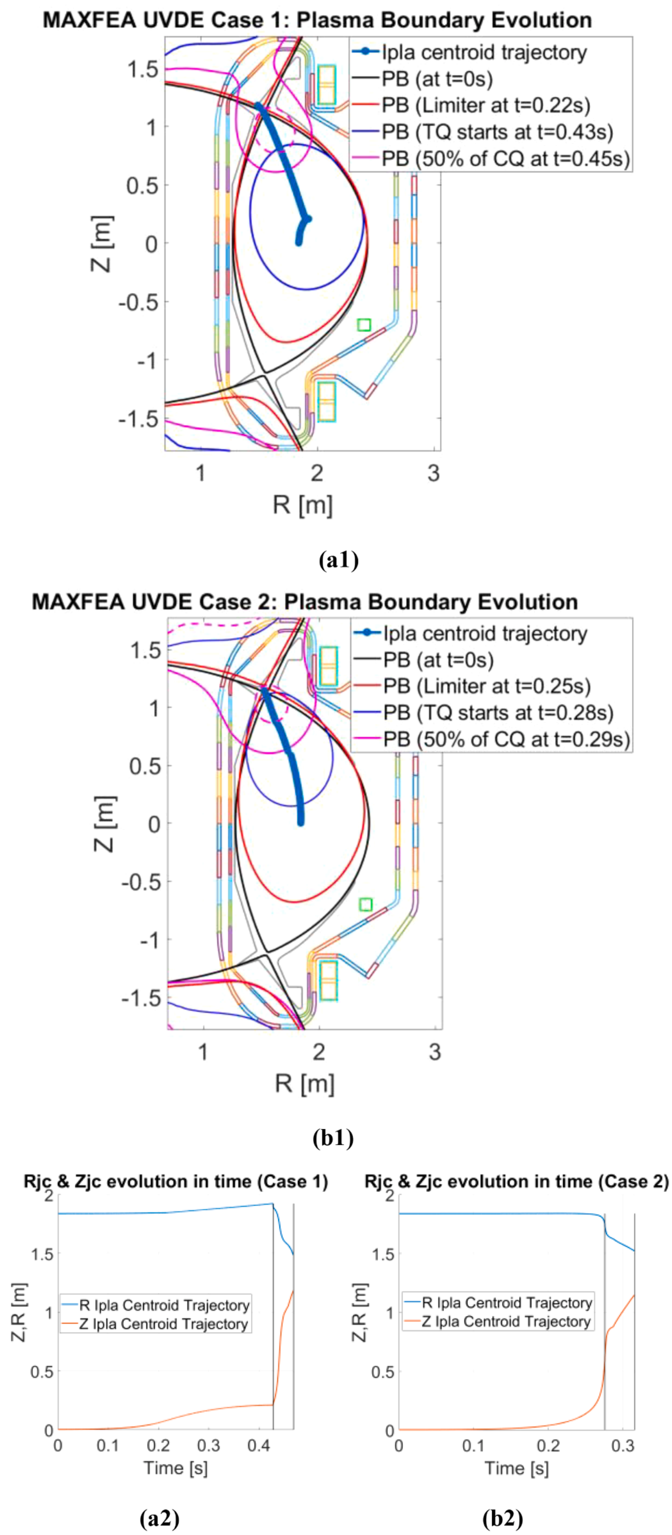

Fig. 6. Plasma movement estimation presenting the plasma centroid evolutions in time (a2)(b2), on poloidal plane (a1)(b1), together with the plasma boundary evolution for Case 1 (a1)(a2) and Case 2 (b1)(b2). In the poloidal plane figures are represented: with the blue trajectory the plasma centroid evolution on poloidal plane, in black the plasma boundary at the equilibrium condition, in red the same when plasma touch the wall, in dark blue at TQ, in magenta at 50 % of CQ. In the time variant figures in blue is represented the radial trajectory of the plasma centroid and the vertical one is shown in red.

plasma current distribution, resulting in variations in coupling effects with passive structures. These differences arise from the varied modelling strategies employed during the VDE phase, as detailed in Section 3.1. In the preceding disruption analysis, the estimated plasma displacement at the onset of the thermal quench is approximately ~0.6 m [4,18]. The inclusion of that result serves to ensure completeness, offering an approximate indication of the order of magnitude of plasma vertical displacement and providing insight into the expected outcomes from SPARC VDE. It is crucial to highlight that slight differences are expected when employing diverse methodologies for such simulations. Nonetheless, the results obtained from MAXFEA simulations instil confidence in asserting the accuracy of the proposed VDE modelling strategy, particularly in terms of plasma vertical dynamics.

The outcomes in terms of eddy currents evolution considering different components are shown Fig. 7. Looking at Fig. 7a1-b1, Case 1 turns out to be the most severe case in terms of eddy currents with ~5.99 MA of induced currents on the VV (purple curves in Fig. 7a1-b1), since the CQ starts from a higher value of the plasma current. EM effects concerning the difference in the vertical movement of two cases are highlighted by observing the eddy trend on VSs (up-down connection in anti-series as suggest the specular curves in Fig. 7a2-b2).

The vertical EM forces (F_z) acting on SPARC components are reported in Fig. 8. Regarding the EM vertical forces (Fig. 8), the most conservative case results to be Case 2. The explanation can be attributed to the fact that in Case 2 it can be found a more unstable plasma at TQ, which influence the halo currents distribution, and the halo force contribution results to be higher (red curves in Fig. 8a-b). Case 2 shows a F_z resultant on the VV structure of about 25 MN upward, consider both the dynamics of VV+VSs induced currents and the halo currents contribution (magenta curve in Fig. 8b). In Case 1, it is observed that the resultant F_z on the VV structure amounts to approximately 22 MN in the upward direction, as depicted by the magenta curve in Fig. 8b. The force contribution of DIVs can be neglected as these components are structurally independent from the vessel. The discrepancies observed in the F_z between the two cases stem from the diverse modelling strategies applied during the VDE phase, as discussed in Section 3.1. A rough comparison can be made by considering the order of magnitude of results from previous disruption studies, which estimated a disruption EM load acting on the vacuum vessel of ~26 MN [4,18]. However, it is important to emphasize that slight differences are anticipated when imposing different conditions and employing diverse methodologies for such simulations, as discussed in [9]. Therefore, the comparison cannot be intended for validation purposes but rather serves as a motivation for completeness. Furthermore, it is important to note that the results obtained in terms of global forces should not be interpreted as a detailed load specification. It is essential to highlight that the primary focus is on the dynamics of the plasma for these simulations, which will serve as input for detailed 3D analyses (see Fig. 1). Here, the 2D total integrated forces are provided for completeness, but more substantial considerations of their trends will be made based on the results of 3D EM analyses.

4. SPARC synthetic disruption database

Having gained confidence in the new model and following the initial application of the proposed disruption modelling strategy to SPARC (as discussed in Section 3), it became possible to explore other cases by collecting 16 additional disrupted scenarios (for a total of 18 cases) to assemble a database of synthetic disruptions. The objective is to prepare predictive disruption simulations as synthetic experiments aimed at providing data for training a subsequent SPARC synthetic diagnostic, as outlined in the introduction. The purpose of this collection is precisely to provide disruption data under various conditions. This involves proposing a series of events with different characteristics, including variations in the plasma vertical evolution during the VDE phase, diverse impositions of TQ at various vertical positions of the plasma, different

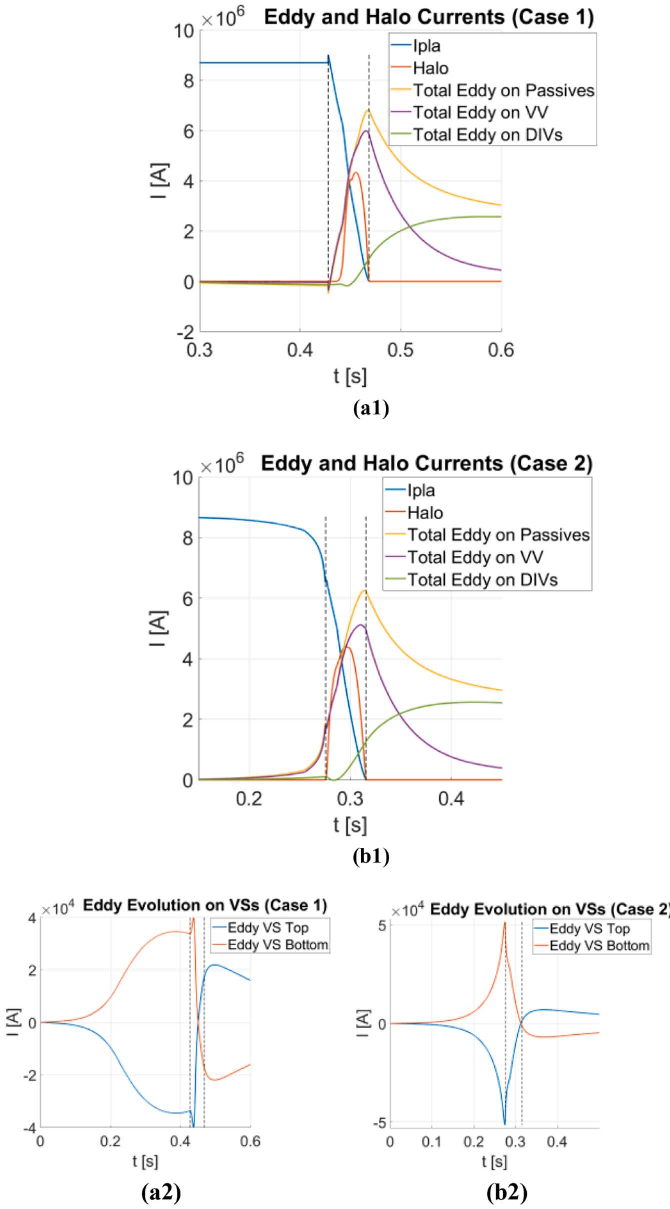

Fig. 7. MAXFEA computed eddy currents trend in time on SPARC components for Case 1 (a1)(a2) and Case 2 (b1)(b2). Graphs in (a1)(b1) show the plasma current and halo currents dynamics (blue and red lines respectively), the evolution of total eddy currents considering all passive structures including the VS and DIV coils (yellow trend), the eddy currents trend on the VV structure (purple curve) and the dynamics of total eddy currents considering the contribute of DIVs induced currents (green trend). Images (a2)(b2) the eddy current evolution (A·Turns) on the top and bottom VS circuits (blue and red evolution) are presented.

CQ and halo current dynamics. The following points aim to provide an explanation of the DB construction strategy and a comprehensive exposition of the parameter ranges used to drive the simulations collected in the database:

1. **Scanning on q_{cyl} at TQ:** as already discussed in Section 3.1, there exists a correlation between q_{cyl} and the vertical displacement of the plasma at the time when TQ occurs. Therefore, exploring a range of q_{cyl} means examining various scenarios in terms of plasma vertical evolution prior to disruption. Again, the determination of both the upper and lower bounds for between q_{cyl} is a matter of assumptions. Typically, the greater the vertical displacement of the plasma before disruption, the higher the total vertical force induced in the structures. In the case of SPARC, the lower limit for q_{cyl} is fixed at 1 (as imposed for Case 1 and Case 2 discussed in Section 3). Instead, the rationale behind setting the upper bound is as follows: experimentally, in most cases, plasma disruptions occur as the plasma begins to strongly interact with the walls, that is often when the plasma begins contacting the wall during its vertical movement (first limiter plasma). This interaction leads to the generation of particles that can migrate into the plasma, triggering a thermal collapse. When the plasma disrupts close to its original position, the event can be categorized as a major disruption (MD or cold-VDE) [8, 23]. However, there is no general rule or clear boundary for the differentiation of all the possible disruption event typologies. In this paper, it was decided to define the beginning of the "VDE domain" as the point when the plasma reaches the value of q_{cyl} corresponding to the first limiter configuration it encounters during its vertical evolution. This serves as upper bound in this context. As a first hypothesis, the scanning in the above-mentioned range was carried out considering evenly spaced points from lower to upper bound: TQ at

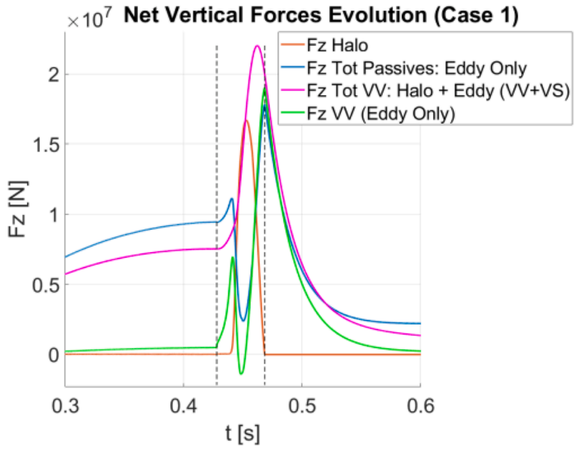

(a)

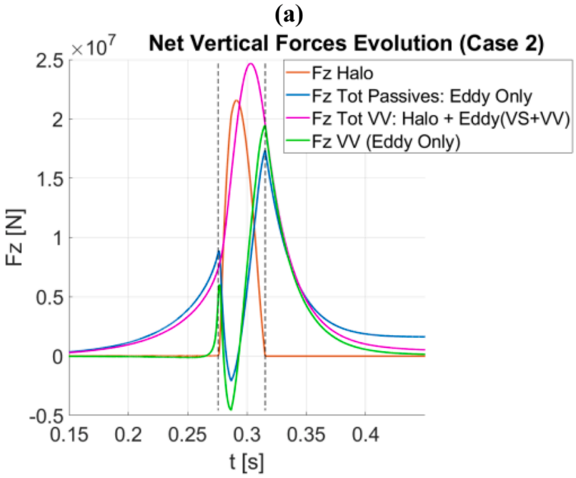

(b)

Fig. 8. MAXFEA 2D vertical forces trend in time on SPARC components for Case 1 (a) and Case 2 (b). Force dynamics due to the halo currents effect is reported in red, the evolution of total forces due to eddy currents considering all passive structures including the VS and DIV coils is in blue, total loads trend act on the VV structure considering the dynamics of VV+VSs total eddy currents and the halo currents contribute is reported in magenta, the F_z acting on the VV with the only eddy contribute is represented by the green trend.

$q_{cyl} = 2.2$, $q_{cyl} = 1.8$, $q_{cyl} = 1.4$, $q_{cyl} = 1.0$. This resulted in a total of 4 different q_{cyl} values at the TQ trigger used for populating the DB.

2. **VDE phase assumptions:** another significant increase in the number of collected cases is attributed to the modelling approach for the VDE phase, specifically with regards to the imposition of either the magnetic flux conservation mode or the magnetic flux normal mode. As extensively discussed in Section 3.1, these two simulative assumptions have a fundamental influence on the dynamics of the plasma during the VDE, effectively doubling the number of cases.
3. **TQ duration:** as reported in Section 3.1, the fast phase of TQ for SPARC has a duration of approximately ∼ 0.1 ms. Moreover, in this type of simulation, it is common practice to assume that all the plasma energy is lost during a single fast phase. Additionally, no scanning on TQ duration was incorporated into the DB construction strategies, given that the actual duration of the TQ has a minor impact on the EM simulations, as detailed in Section 3.1.
4. **CQ duration:** another operational space covered in the DB is correlated with the duration of the CQ, considering the upper and lower design bound explained in Section 3.1: the DB contains 8 UVDE with a fast CQ duration of ∼3.2 ms and 8 slow UVDE with a CQ duration of ∼40 ms, including Case 1 and 2.
5. **Halo current modelling approach**: present understanding of disruption physics and halo current phenomenology makes comprehensive predictive simulations difficult and affected by strong uncertainties. Hence, codes like MAXFEA adopt a "practical approach", where the behaviour of halo during plasma evolutions is determined by specific input parameters that allow for control over the halo region and current evolution. Various definitions exist in the literature for characterizing the halo current region during plasma transients. Recently, within the DEMO disruptions group, a decision has been made to adopt the following definition for the width of the halo region, denoted as w. Fig. 9 provides a qualitative representation of w to aid in understanding the argumentation.

$$w(t) = \frac{\psi_l - \psi_b}{\psi_a - \psi_b} \tag{6}$$

where ψ_l, ψ_b and ψ_a represent the poloidal flux function taken at the defined boundaries depicted in Fig. 9. The specific profiles of $w(t)$ and $I_{pla}(t)$ serve as inputs for these simulations. Recent works within the DEMO disruptions group highlight that the choice of $w(t)$ and $I_{pla}(t)$ can lead to diverse evolutions during the CQ concerning various parameters, such total halo current, plasma shape, and components wetted by the halo current, influencing the EM loads especially on the in-vessel components. However, due to the absence of precise physics guidelines, the alternative is to explore a range of different $w(t)$ and $I_{pla}(t)$ profiles. This approach aligns with the planned implementation to further extend the database in the future, contingent upon its relevance from both engineering and physics perspectives. However, for these simulations, specific values for $w(t)$ and $I_{pla}(t)$ have been set to achieve the following objectives:
   - Obtaining a halo current peak equivalent to 50 % of the initial plasma current in cases where $q_{cyl} = 1$ [4,18]. This represents an engineering limit based on [23]. This is a very unlikely scenario, considering that the cumulative fraction of events that exceed this value is less than 3 % [23].
   - Ensuring that the trend of the halo fraction aligns with observations from [23], which indicate that the poloidal halo current is strongly influenced by the edge safety factor, with lower safety factors resulting in a larger fraction of poloidal halo current.

Fig. 10 shows a qualitative preview of disruptions DB, excluding Case 1 and 2 extensively described in Section 3. Additionally, Table 3 contains a summary aimed at outlining the simulation strategies for each case and the corresponding main outcomes obtained (with reference to Fig. 10).

Going into detail about the DB contents (Fig. 10), the cases collected

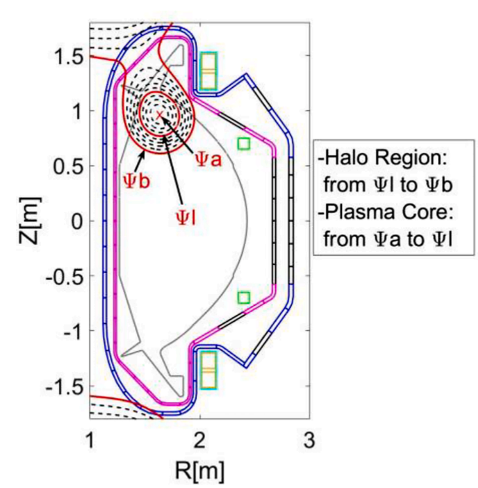

Fig. 9. MAXFEA halo current modelling approach.

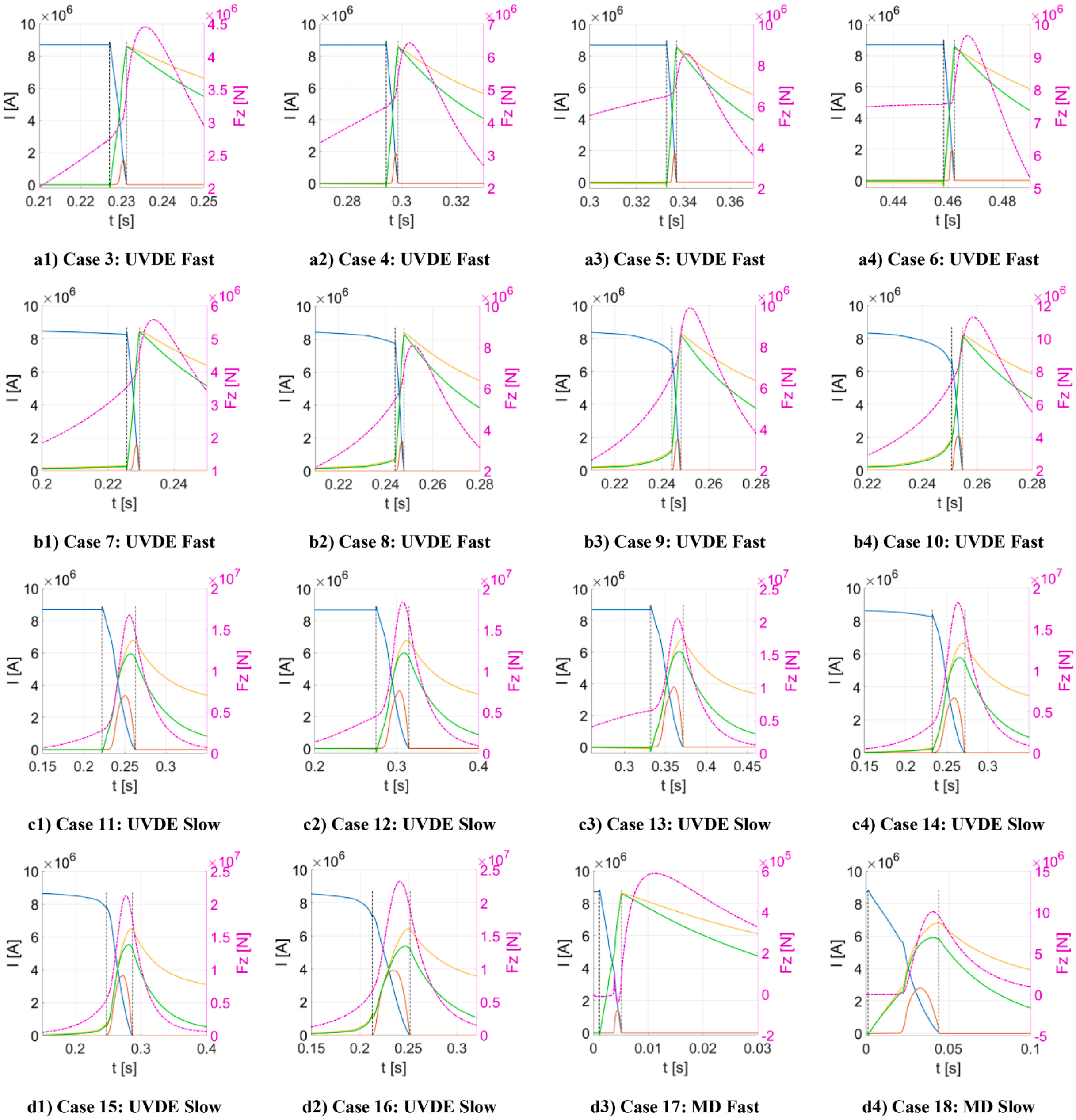

Fig. 10. A semi-qualitative preview of SPARC synthetic disruption DB obtained numerically with MAXFEA code. For each case the following outcomes are reported: plasma current and halo currents (blue and red lines respectively), total eddy currents considering all the passive structures in the model (yellow trends), the eddy currents on the VV structure (green curves), total loads acting on the VV structure (magenta dotted trends, refers to right ordinate axis) considering the contribute of halo and eddy on components structurally supported by the VV (eddy from the VV+VSs).

are subsequently exposed. The DB contains 8 UVDE with a fast CQ duration of ∼4 ms and 8 slow UVDE with a CQ duration of ∼40 ms, including Case 1 and 2. Fast UVDEs from Case 3 to Case 6 (Fig. 10a1-a2-a3-a4) and slow UVDEs from Case 11 to Case 13 (Fig. 10c1-c2-c3) are simulated by keeping the plasma current constant up to TQ (flux normal mode described in SubSection 3.1). In fast UVDEs from the Case 7 to the Case 10 (Fig. 10b1-b2-b3-b4) and in slow UVDEs from the Case 14 to the Case 16 (Fig. 10c4-d1-d2) the plasma current is characterized with a decreasing trend up to TQ (flux conservation mode described in Sub-Section 3.1). In this way it can be imposed a differentiation between cases in terms of plasma dynamics during vertical displacement. In addition, another differentiation between the cases concerns the method to impose TQ. Similar to Case 1 and Case 2, TQ is imposed when q_{cyl} reaches a limit value. In the DB, different q_{cyl} critical values are considered, taking into account the range from 2.2 (when the plasma touches the wall) to 1 (similar to Case 1 and Case 2). Specifically, for Case 3, 7, 11 and 14 the critical q_{cyl} value is ∼ 2.2; for Case 4, 8, 12 and 15 is ∼ 1.8; for Case 5, 9, 13 and 16 is ∼ 1.4; for Case 6 and 10 is ∼ 1. In this way it is possible to obtain a number of events with different stability conditions and different plasma positions at TQ.

Finally, the disruption DB includes two cases of MD with a central plasma at TQ [8,23]. These two events refer to Case 17 and Case 18 (Fig. 10d3-d4), in which TQ is imposed a few ms after the start of the simulation with an abrupt β_p perturbation. Then the plasma moves radially touching the inboard wall and CQ (fast in Case 17 and slow in Case 18) is imposed immediately after TQ. The different conditions among events in terms of plasma dynamics during vertical displacement, typologies of event and stability conditions at TQ; generate a

Table 3
DB summary table reassuming the simulation strategies for each case (VDE+MD), such as: TQ trigger at different q_{cyl}, different flux condition during the VDE phase (normal “No” or conservation “Co”), CQ duration (fast "F" or slow "S"). In addition, an important focus on halo currents fraction (Fr_{halo}) is presented (peak as a percentage of initial I_{pla} [23]), together with the values of vertical plasma current centroid coordinates (Z_{jc}) at TQ. Table shows for completeness total eddy currents peaks ($I_{eddy,max}$) and vertical forces ($F_{z,max}$) peaks acting on the VV structure for each case. As for the forces, contributes from VV+VSs total eddy currents and halo currents are considered (Fig. 10 for entire time evolutions).

	VDE																MD	
Cases	1	2	3	4	5	6	7	8	9	10	11	12	13	14	15	16	17	18
VDE Phase (Flux Mode)	No	Co	No	No	No	No	Co	Co	Co	Co	No	No	No	Co	Co	Co	–	–
CQ (Fast/Slow)	S	S	F	F	F	F	F	F	F	F	S	S	S	S	S	S	F	S
TQ Trigger (q_{cyl}) [-]	1	1	2.2	1.8	1.4	1	2.2	1.8	1.4	1	2.2	1.8	1.4	2.2	1.8	1.4	–	–
Z_{jc} @TQ [cm]	∼ 21	∼ 60	∼ 10	∼ 14	∼ 18	∼ 21	∼ 15	∼ 27	∼ 42	∼ 60	∼ 10	∼ 14	∼ 18	∼ 15	∼ 27	∼ 42	∼ 0	∼ 0
Fr_{halo} [%]	50	50	18	21	22	23	18	21	22	23	39	42	44	39	42	44	16	32
$I_{eddy,max}$ [MA]	6.0	5.1	8.6	8.5	8.6	8.6	8.4	8.3	8.2	8.1	5.9	6.0	6.0	5.8	5.5	5.4	8.6	5.9
$F_{z,max}$ [MN]	22.0	24.7	4.5	6.4	8.6	9.7	5.6	8.1	9.9	11.3	16.8	18.4	20.5	18.2	21.3	23.2	0.6	10.1

differentiation from the point of view of eddy and halo current entities, distribution and force contributions (see Fig. 10 and Table 3)

Looking at Table 3, significant observations can be made regarding the relationship between simulation strategies and the obtained results in terms of plasma evolution. Particularly, the effect of the approach used to simulate the VDE phase on the plasma vertical displacement up to TQ is clearly evident. Comparing two analogous cases sharing the same CQ dynamics and TQ trigger (e.g., Case 3 and Case 7), similar behaviour to that discussed in detail in Section 3 is observed. The plasma undergoes different EM expansion due to the differences in the variations within the evolution of the internal current density distribution, which impacts the coupling with passive structures. Consequently, cases simulated with a flux conservation approach are more compressed towards the inboard with the plasma that reach greater Z_{jc} at the TQ, as expected (Section 3.1). A further interesting observation can be made when comparing cases with the same assumptions regarding VDE phase modelling and CQ duration but different TQ triggers. For example, comparing Case 3, Case 4, Case 5, and Case 6, one can observe an increasing trend in Z_{jc} as the value of q_{cyl} decreases. This trend is expected as a lower q_{cyl} value delays the TQ phase, allowing the plasma more time to vertically displace during the VDE phase. Indeed, as previously noted, a greater vertical displacement of the plasma before disruption results in a higher total vertical force induced in the structures, consequently affecting plasma stability. Since halo currents have a stabilizing effect in these codes, a higher Z_{jc} at TQ corresponds to increased plasma instability, which is compensated by a higher halo fraction, as observed in Table 3.

As previously mentioned, the primary emphasis in this context is on the dynamics of the evolutions, which will be utilized as input for future steps. This inherently involves a heightened focus on halo dynamics and on the modelling of plasma evolution, as detailed in Section 3. Consequently, the 2D total integrated force outcomes are included for completeness and should be regarded as preliminary results. A more in-depth analysis of their trends can be conducted once the results of the 3D EM analyses become available.

Conclusions and next steps

The aim of this study was to utilize the MAXFEA 2D equilibrium code to construct a synthetic disruption database through numerical disruption simulations. These simulations explored various sets of characteristic parameters and plasma dynamic conditions. The SPARC 2D FEM model was implemented, and the disruption modelling strategy was applied to SPARC, leveraging existing disruption evidence for the machine [2,4,18]. Following the successful application of the proposed disruption modelling methodology, a total of 18 cases were collected to assemble the synthetic disruptions database. One of the primary objectives of this work is to address the gap in accurate numerical modelling of SPARC disruption plasma dynamics, while exploring various parameters of interest.

The next steps will involve the development of a synthetic diagnostics system for SPARC, commencing with the utilization of the 2D disruption simulations collected. This will be followed by leveraging the MAXFEA-ANSYS coupling methodology to provide 3D EM and structural assessments as an intermediate step. This innovative approach seeks to indirectly estimate the displacement and strain field of components, thereby deriving stress measurements crucial for characterizing the SPARC VV. The ultimate goal is to suggest the implementation of "indirect" displacement or deformation diagnostics at accessible points on the machine, facilitating real-time reconstruction of the machine overall deformation. This reconstruction process relies on an understanding of the modal shapes that describe the dynamic behaviour of the structure. Modal reconstructions offer a computational advantage, requiring fewer resources compared to FEM analyses. However, their effectiveness relies on selecting appropriate vibration modes, which is heavily influenced by the load conditions. Constructing a synthetic database enables training ML algorithms to select modes that accurately represent the machine response. This database aims to simulate real load conditions experienced by the tokamak vessel, enhancing our understanding of its behaviour under various scenarios. Modal reconstruction has been extensively studied in the aeronautical field and in fluid-structure interaction [16], but its application in the fusion field is relatively novel. Therefore, this represents an innovative area of research with promising potential.

Credit authorship contribution statement

M. Scarpari: Writing – review & editing, Writing – original draft, Visualization, Validation, Software, Methodology, Investigation, Formal analysis, Data curation, Conceptualization. **R. Lombroni:** Writing – review & editing, Writing – original draft, Visualization, Validation, Software, Methodology, Investigation, Formal analysis, Data curation, Conceptualization. **A. Mele:** Writing – review & editing, Writing – original draft, Visualization, Validation, Software, Methodology, Formal analysis, Data curation, Conceptualization. **S. Carusotti:** Validation, Software, Methodology, Formal analysis, Conceptualization. **S. Minucci:** Writing – review & editing, Writing – original draft, Methodology, Conceptualization. **G. Liuzzo:** Writing – review & editing, Validation, Software, Methodology, Formal analysis. **M. Notazio:** Validation, Software, Methodology, Formal analysis, Conceptualization. **V. Riccardo:** Writing – review & editing, Supervision, Resources, Project administration, Conceptualization. **G. Calabrò:** Writing – review & editing, Supervision, Resources, Project administration, Funding acquisition, Conceptualization. **P. Fanelli:** Writing – review & editing, Supervision, Resources, Project administration, Funding acquisition, Conceptualization.

Declaration of competing interest

The authors declare that they have no known competing financial interests or personal relationships that could have appeared to influence the work reported in this paper.

Data availability

The data that has been used is confidential.

Acknowledgments

The work was supported by Commonwealth Fusion Systems. The authors are very grateful to Commonwealth Fusion Systems for providing data of SPARC tokamak.

References

[1] B.N. Sorbom, et al., ARC: A compact, high-field, fusion nuclear science facility and demonstration power plant with demountable magnets, Fusion Engineering and Design 100 (2015) 378–405, https://doi.org/10.1016/j.fusengdes.2015.07.008.
[2] R. Sweeney, et al., MHD stability and disruptions in the SPARC tokamak, Plasma Phys. 86 (2020) 865860507, https://doi.org/10.1017/S0022377820001129R.
[3] F.C. Schuller, Disruptions in tokamaks, Plasma Phys. Control. Fusion 37 (11A) (1995), https://doi.org/10.1088/0741-3335/37/11A/009.
[4] V. Riccardo and the SPARC Team, "Disruptions Loads in SPARC", Second Technical Meeting on Plasma Disruptions and their Mitigation, ITER Headquarters, July 2022. https://conferences.iaea.org/event/281/contributions/24400/attachments/13000/20067/Riccardo_SPARC_220719.pdf.
[5] R.A. Tinguely et al. 2021 Nucl, Fusion 61 124003. doi:10.1088/1741-4326/ac31d7.
[6] P. Barabaschi, "The MAXFEA code", Proc. Plasma Control, Technical Meeting (Naka, Japan, April 1993).
[7] R. Lombroni, et al., Using MAXFEA code in combination with ANSYS APDL for the simulation of plasma disruption events on EU DEMO, Fusion Eng. Des. 170 (March) (2021) 112697, https://doi.org/10.1016/j.fusengdes.2023.113611.
[8] G. Sias, et al., Inter-machine plasma perturbation studies in EU-DEMO relevant scenarios: lessons learnt for EM forces prediction during VDEs, Nucl. Fusion (2022), https://doi.org/10.1088/1741-4326/ac544b.
[9] F. Maviglia, et al., Integrated design strategy for EU-DEMO first wall protection from plasma transients, Fusion Eng. Des. 177 (2022) 113067, https://doi.org/10.1016/j.fusengdes.2022.113067.
[10] Martinez 2013, "ITER Vacuum vessel load specification", ITER_D_2F52JY v3.3.
[11] V. Rozov, et al., Multi-scenario evaluation and specification of electromagnetic loads on ITER vacuum vessel, Fusion Engineering and Design 89 (2014) 1826–1831, https://doi.org/10.1016/j.fusengdes.2014.03.003.
[12] G.A. Spagnuolo, et al., Fusion Engineering and Design 157 (2020) 111657, https://doi.org/10.1016/j.fusengdes.2020.111657.
[13] F. Giorgetti, et al., Vertical Displacement Events Analysis Using MAXFEA Code in Combination with ANSYS APDL in the Final Design Stage of the DTT Vacuum Vessel, Fusion Eng. Des. 184 (August) (2022) 113273, https://doi.org/10.1016/j.fusengdes.2022.113273.
[14] R. Lombroni, et al., Use of MAXFEA-ANSYS Tool to Study the Electro-Magnetic Behaviour of the New ST40 Inner Vacuum Chamber Proposal during a Plasma VDE, Fusion Eng. Des. 192 (March) (2023) 113611, https://doi.org/10.1016/j.fusengdes.2023.113611.
[15] S. Carusotti, Structural Behaviour Characterization of ST40 Inner Vacuum Chamber (IVC2) during a Plasma VDE Using ANSYS Workbench, Fusion Eng. Des. 192 (July) (2023) 113772, https://doi.org/10.1016/j.fusengdes.2023.113772.
[16] P. Fanelli, et al., Structural health monitoring of cylindrical bodies under impulsive hydrodynamic loading by distributed FBG strain measurements, Measurement Science and Technology 28 (2) (2017) 024006, https://doi.org/10.1088/1361-6501/aa4eac.
[17] A. Coutlis, et al., Measurement of the open loop plasma equilibrium response in TCV, Nucl. Fusion 39 (1999) 663, https://doi.org/10.1088/0029-5515/39/5/307.
[18] Private communications with SPARC team (2023).
[19] A.J. Creely, et al., Overview of SPARC tokamak, J. Plasma Phys. 86 (2020) 865860502, https://doi.org/10.1017/S0022377820001257.
[20] S.L. Chen, F. Villone, et al., Equivalent Axisymmetric Plasma Response Models of EAST, Plasma Phys. Controlled Fusion 58 (2) (2016) 025017, https://doi.org/10.1088/0741-3335/58/2/025017.
[21] J. Wesson, D.J. Campbell, Tokamaks, Volume 149, Oxford university press, 2011.
[22] E.A. Lazarus, J.B. Lister, G.H. Neilson, Control of the vertical instability in tokamaks, Nuclear Fusion 30 (1) (1990) 111, https://doi.org/10.1088/0029-5515/30/1/010.
[23] N.W. Eidietis, et al., The ITPA disruption database, Nucl. Fusion 55 (6) (2015) 63030, https://doi.org/10.1088/0029-5515/55/6/063030.
[24] S.N. Gerasimov, et al., Nucl, Fusion 54 (073009) (2014), https://doi.org/10.1088/0029-5515/54/7/073009.
[25] S.N. Gerasimov, et al., 2020 Nucl, Fusion 60 (066028) (2020), https://doi.org/10.1088/1741-4326/ab87b0.
[26] ITER I.O., Load specifications (LS), ITER ref. 222QGL_v6_0 (2012).